X-Ray Photoelectron Diffraction in the Backscattering Geometry: A Key to Adsorption Sites and Bond Lengths at Surfaces

T. Greber, J. Wider, E. Wetli, and J. Osterwalder

Physik-Institut, Universität Zürich-Irchel, Winterthurerstrasse 190, CH-8057 Zürich, Switzerland

(Received 7 May 1998)

For a well-characterized (2×1)-1O adsorbate phase of oxygen on rhodium (111) we have identified photoelectron interference fringes in the backscattering geometry for O 1*s* adsorbate emission at 723 eV kinetic energy. Although these features are weak, they show up as characteristic rings covering large regions of the full hemispherical photoelectron diffraction pattern. They represent the situation of a simple two-atom electron interferometer and yield directly the most relevant information on the adsorbate geometry such as the adsorption site, the adsorbate-substrate bond length, and the bond angle. [S0031-9007(98)06936-1]

PACS numbers: 68.35.Bs, 61.14.Qp, 82.65.Jv, 82.80.Pv

The precise determination of the adsorption geometry of atoms, molecules, and molecular fragments on metal surfaces is one of the keys to understanding the mechanisms of catalytic activity and selectivity [1]. Low-energy electron diffraction (LEED) is still considered to be the prime experimental technique to provide this type of information, with atomic positions typically determined to an accuracy of better than a tenth of an angstrom [2]. Photoelectron diffraction is a related technique which has one very attractive feature: The excitation process makes it selective to an elemental species on the surface [3,4]. From the photoelectron spectrum of the sample one can select the signal from a specific core level and record diffraction effects either as a function of emission angle—x-ray photoelectron diffraction (XPD)—or as a function of emission energy—energy-scanned photoelectron diffraction. Over the last few years, the latter mode has been very successfully applied to measuring bonding sites and bond distances of adsorbed molecules [4], either by running model calculations or more recently by direct methods that couple the information of energy scans along a few directions [5,6].

It is the angular distribution of photoelectrons that carries the most intuitive information on the local geometry around the photoemitting atom: The scattering processes with individual neighbor atoms have a characteristic form factor (Fig. 1) which—for energies of a few hundred eV and higher—is strongly peaked in the forward direction ($\theta_s = 0°$) [7]. Scattering at higher angles is more uniform while there is again a slight enhancement near the backscattering geometry ($\theta_s = 180°$). This latter effect is more pronounced for lower electron energies and for scatterers with higher atomic numbers Z. The strong forward scattering enhancement can lead to high anisotropies in the photoemission signal—defined as $A = (I_{FS} - I_0)/I_{FS}$ where I_{FS} is the intensity along the emitter-scatterer direction and I_0 is some average intensity away from this direction—with measured values reaching more than 50% [8]. These pronounced signals have been exploited successfully to identify bond directions within adsorbed molecules [9,10] and molecular orientation [11], as well as the atomic structure in ultrathin films [12]. For studying the bonding geometry of an adsorbate relative to the substrate, such signals are not available, because the emitter-scatterer directions point into the crystal.

In energy-scanned photoelectron diffraction one exploits the enhanced backscattering in order to have strong interference effects. The question now is as follows: Can one find such backscattering processes in XPD and extract structural information from them as directly as from forward scattering peaks? The answer is—of course—yes, but one has to push the experiment along two directions: Complete angular distributions of photoelectrons have to

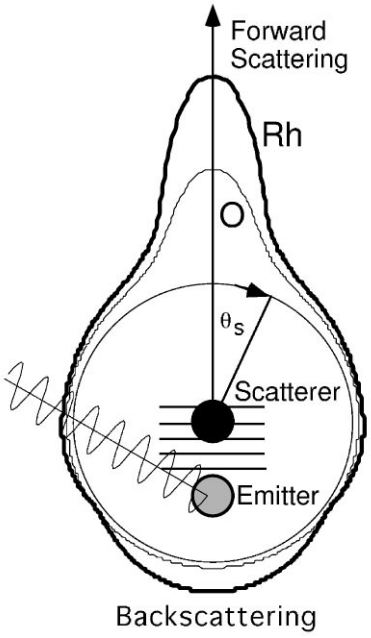

FIG. 1. Polar diagram of the scattering amplitude of an electron plane wave of 723 eV kinetic energy scattering off a Rh atom (thick line) and an oxygen atom (thin line). The circle represents zero amplitude.

 0031-9007/98/81(8)/1654(4)$15.00

be measured in order to discriminate specific scattering processes using simple symmetry arguments, and one needs data of sufficient statistical accuracy in order to measure anisotropy values of less than 5% with confidence.

In this Letter we present full hemispherical XPD data of O 1*s* emission from a well defined adsorbate phase of oxygen on Rh(111). Schwegmann *et al.* [13] have characterized a saturated (2×1)-1O phase of half a monolayer oxygen coverage, occurring in three rotated domains. Using LEED, they have identified the threefold hollow fcc site to be the stable adsorption site, with a spacing of 1.23 ± 0.05 Å between the oxygen and the top Rh layer. We have prepared this phase by exposing a clean Rh(111) surface to 10 Langmuir of O_2 at room temperature. The measured LEED pattern showed the characteristic (2×2) periodicity which is consistent with the three-domain (2×1) structure. XPD patterns were measured in the same Vacuum Generators ESCALAB 220 spectrometer, using our customized and computer-controlled sample goniometer [14]. In Fig. 2 we present patterns of Rh $3d_{5/2}$ emission—containing the information on the crystal directions—and O 1*s* emission—containing the adsorbate site information. The plots consist of roughly 4000 pixels, each of which represents a set of polar (θ) and azimuthal (ϕ) emission angles, plotted in stereographic projection. The gray scale value of each pixel is linearly related to the corresponding photoemission signal, all of which are recorded sequentially. In producing the O 1*s* plot, the spectral background had to be carefully subtracted from the O 1*s* signal, because it is well known to carry the angular signature of the higher kinetic energy Rh $3p_{1/2}$ peak which is only 8 eV away [15]. Recording one complete O 1*s* pattern takes typically 5 h. At room temperature we found that the surface oxygen layer became gradually depleted due to oxygen desorption after reaction with residual gas (mostly H_2 and CO) at a pressure of typically 5×10^{-10} mbar. Cooling the crystal to 190 K during the measurement proved to keep the adsorbate layer more or less stable, with a small contribution due to CO accumulating over the measuring time.

Before discussing the O 1*s* XPD pattern and how it relates to the oxygen bonding geometry, it is instructive to visualize diffraction patterns of simple emitter-scatterer configurations relevant for adsorbate geometries. In Fig. 3a we show the pattern produced by an oxygen atom slightly below the surface, calculated with the single-scattering cluster (SSC) formalism [3,16]. Scattering by only one single Rh atom in the surface layer is considered. The axial geometry of this two-atom configuration produces a characteristic interference pattern, with a strong forward scattering maximum along the bond axis, and rings of constructive and destructive interference whenever the wave scattered off the Rh atom is in or out of phase with the unscattered wave. The anisotropy of the forward scattering peak is here 93% if the adjacent minimum is taken for the reference intensity I_0, or 75% if I_0 is taken to be the average intensity over the first two interference fringes (see Fig. 3a). For higher oxygen coverages, we were able to identify a subsurface species of oxygen and to detect concentrations as low as 5% of a monolayer thanks to these strong anisotropies [17].

In Fig. 3b we have moved the oxygen atom out of the surface into a position which corresponds to the O-Rh nearest-neighbor geometry found by Schwegmann *et al.*

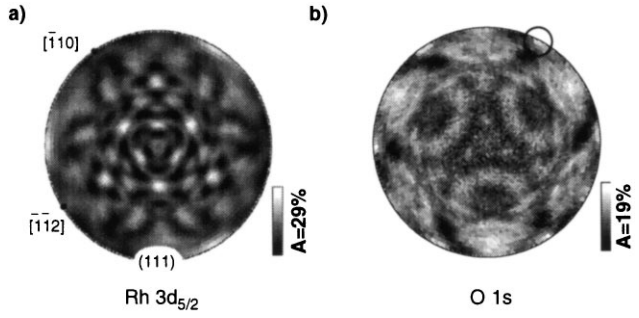

FIG. 2. Measured photoelectron diffraction patterns for (a) Rh $3d_{5/2}$ emission ($E_{\mathrm{kin}} = 947$ eV) from a clean Rh(111) surface, and for (b) O 1*s* emission ($E_{\mathrm{kin}} = 723$ eV) from a (2×1)-1O/Rh(111) surface. The data are stereographically projected. Intensities are represented in a linear gray scale with gray bars indicating the overall anisotropy $A = (I_{\max} - I_{\min})/I_{\max}$ for each pattern. The circle in (b) indicates one oxygen-oxygen forward scattering direction (see text).

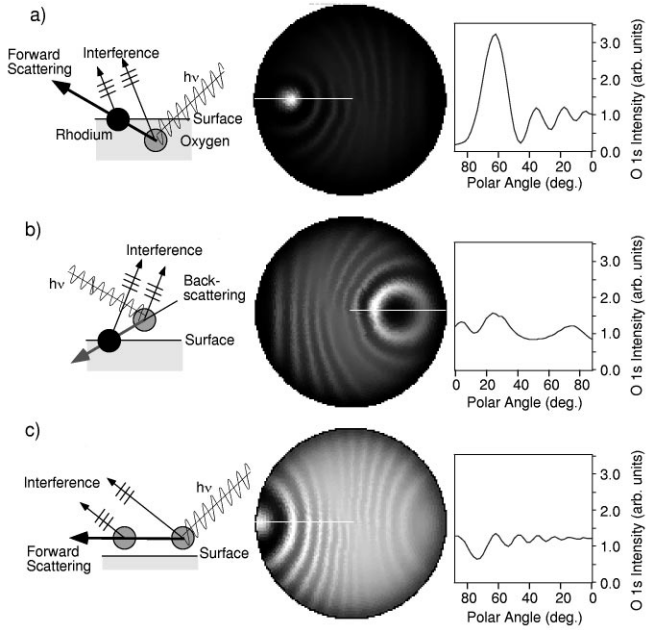

FIG. 3. Single-scattering cluster calculations for O 1*s* emission at $E_{\mathrm{kin}} = 723$ eV for selected two-atom geometries: (a) Subsurface oxygen–surface Rh layer; (b) adsorbed oxygen–surface Rh layer; and (c) oxygen-oxygen adsorbate scattering. The scattering geometries are illustrated for each case. Full XPD patterns are shown as well as a polar intensity scan along one high-symmetry direction (white line) which quantifies the absolute anisotropies.

[13]. Following our expectations the forward scattering peak has moved below the surface and is no longer visible for this geometry. Instead, we identify the 180° backscattering direction by its axial symmetry. A bright circle represents a fringe of constructive interference of the directly emitted O 1s photoelectron wave and the wave backscattered by the Rh neighbor. The axis of the corresponding scattering cone is centered at a polar angle of 50°. We assign this circle to 11th order diffraction, where the fringes are counted from the forward scattering direction (zero order). This backscattering fringe is stronger than the lower order fringes because of the enhanced form factor in near-backscattering directions for Rh (Fig. 1). From this calculation we find an anisotropy of 25%–40% for this ring, depending on how we define I_0.

There exists one further predominant scattering geometry for periodic high-coverage adsorbate structures: Equivalent adsorbate atoms in adjacent surface unit cells represent forward scattering geometries with the peak lying in the surface plane. Because these peaks have a full width at half maximum of typically 20°, they lead to strong measurable anisotropies (30%–50% for the case of Fig. 3c) in a polar angle range of $\theta_s = 80°–90°$, and with a characteristic symmetry as depicted in Fig. 3c.

After having sharpened our eyes to characteristic symmetry features we now proceed to discuss the experimental O 1s pattern of Fig. 2b. In doing this one should remember that the experimental situation presents all the discussed geometries at the same time and that the scattering processes superpose coherently. Nevertheless we can recognize six equidistant forward scattering peaks for grazing emission, i.e., along the rim of the plot, which indicate the oxygen-oxygen directions within the adsorbate lattice. The associated interference fringes are strongly entangled with other scattering processes, and only the first-order fringe shows up at some places.

We now focus on a more obvious set of features visible in these data: There are three rings of enhanced intensity, surrounded by circular intensity depressions, which are arranged in a threefold fashion spanning together a large portion of the full pattern. The appearance of these rings is strongly reminiscent of the backscattering fringe of Fig. 3b, although the fringes are here modulated and intersected by other scattering features. Nevertheless, the center positions and the ring diameters are well defined in the data. From these two properties we obtain the information on the bonding site: The ring center is related to the direction of an adsorbate-substrate nearest-neighbor bond, while the ring diameter is characteristic of the path length difference of the scattered and unscattered waves plus a scattering phase shift. It is thus a measure for the adsorbate-substrate bond length. The phase condition for constructive interference is

$$kr(1 - \cos\theta_s) + \Psi_s(\theta_s) = 2\pi n\,, \qquad (1)$$

where k is the magnitude of the photoelectron wave vector, r the bond length, $\Psi_s(\theta_s)$ the scattering phase shift, and n the diffraction order. In the backscattering region $\Psi_s(\theta_s)$ is, to a good approximation, constant [7], and the dispersion of the fringe angle with bond distance becomes

$$\frac{d\theta_s}{dr} = -\frac{1 - \cos\theta_s}{r\sin\theta_s}\,. \qquad (2)$$

At a scattering angle of 155° a bond length variation $\Delta r/r$ of $\pm 1\%$ thus corresponds to an angular shift $\Delta\theta$ of $\pm 2°$ which can readily be measured for a diffraction order of ≈ 10. This indicates that XPD is sensitive to bond length changes of the order of ± 0.02 Å.

In order to illustrate these arguments we have performed SSC calculations for simple four-atom clusters containing one oxygen emitter in a threefold hollow site formed by three Rh atoms. In Figs. 4a–4d four patterns are shown which are representative for oxygen adsorbed in the fcc

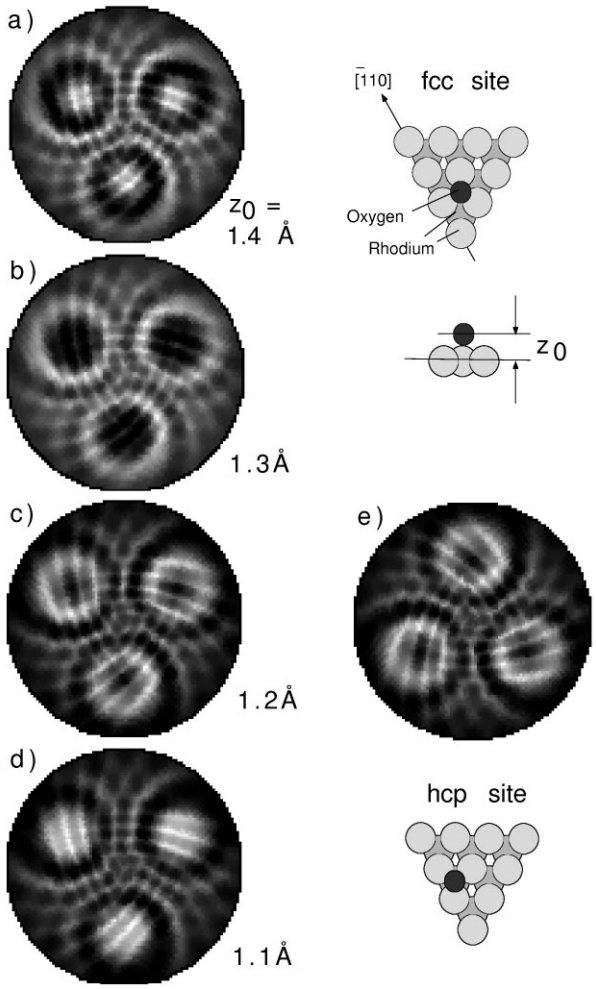

FIG. 4. Single scattering cluster calculations for O 1s emission at $E_{\rm kin} = 723$ eV for simple four-atom clusters representing one oxygen atom and three nearest-neighbor Rh atoms forming a threefold hollow adsorption site. In (a)–(d) the O atom occupies the fcc site at various layer spacings z_0 (see illustration), while (e) shows the adsorption in the hcp site.

site with various bond distances, while Fig. 4e presents one calculation for hcp site adsorption. On the (111) surface of an fcc crystal these two sites have equivalent oxygen nearest-neighbor geometries which are only distinguished by the second Rh layer. We know the absolute orientation of the substrate lattice from the Rh $3d_{5/2}$ data of Fig. 2a, and the calculated patterns in Fig. 4 are plotted to match the orientation of those data. From the comparison with the measured O 1*s* pattern (Fig. 2b), the fcc site immediately leaps to the eye as the stable adsorption site for this system. We further confirm that 0.1 Å steps in layer spacing produce strong effects in the appearance of the backscattering fringes. The intensity in the center of these fringes is either a minimum or a maximum as fringes move away from the backscattering direction with increasing bond length. From a *R*-factor analysis between SSC calculations and experiment an equilibrium O-Rh layer spacing z_0 of 1.21 ± 0.02 Å is found. This confirms the LEED value of 1.23 ± 0.05 Å [13]. Moreover, in the present geometry the bond length is coupled to the bond angle, since we move the O atom vertically in the fcc adsorption site. The position of the fringe thus serves as an independent measure for the bond length, again confirming the value found above. We also see that the mutual presence of three backscatterers produces interference effects that modulate the intensity along the fringes.

We have established the value of backscattering XPD data from adsorbates for direct determination of adsorption site and bond length. Although this effect has been predicted [18] it was not clearly observed so far. First of all we note that the measured fringe anisotropy is very low, less than 5%. If one does not have the complete hemispherical data set, where the fringes can be identified by their mere shape, they are hardly noticeable. However, such fringes have not been observed on adsorbate data of similar quality taken for Na adsorbates on Al surfaces [12], nor in similar cases. We can isolate two important factors that benefit the observation of backscattering fringes: The presence of a high-*Z* substrate with a scattering form factor rising substantially in the backscattering direction, and a low surface temperature during the measurement. Thermal effects in photoelectron diffraction are typically described by using Debye-Waller factors for each scattering path [3]. For backscattering, the momentum change is highest, and therefore these processes suffer the strongest suppression with rising temperature.

In summary, we have identified characteristic photoelectron diffraction features in the backscattering direction for adsorbate emission at 723 eV kinetic energy, corresponding to 11th order diffraction. Their direct observation in the XPD pattern makes them a particularly attractive feature for adsorbate studies, serving as a photoelectron interferometer that yields bonding geometries and bond lengths to an ultimate precision of ± 0.02 Å.

We thank W. Deichmann, P. Schwaller, and T. J. Kreutz for their assistance with the experiment. This work was supported by the Swiss National Science Foundation.

[1] G. A. Somorjai, *Introduction to Surface Chemistry and Catalysis* (John Wiley and Sons, New York, 1994).
[2] P. R. Watson, M. A. Van Hove, and K. Hermann, J. Phys. Chem. Ref. Data, Monograph No. **5**, 1 (1994).
[3] C. S. Fadley, in *Synchrotron Radiation Research: Advances in Surface Science*, edited by R. Z. Bachrach (Plenum, New York, 1989), Chap. 9.
[4] D. P. Woodruff and A. M. Bradshaw, Rep. Prog. Phys. **57**, 1029 (1994).
[5] R. Dippel, D. P. Woodruff, X.-M. Hu, M. C. Asensio, A. W. Robinson, K.-M. Schindler, K.-U. Weiss, P. Gardner, and A. M. Bradshaw, Phys. Rev. Lett. **68**, 1543 (1992).
[6] Ph. Hofmann, K.-M. Schindler, S. Bao, A. M. Bradshaw, and D. P. Woodruff, Nature (London) **368**, 131 (1994).
[7] M. Fink and A. C. Yates, At. Data **1**, 385 (1970); M. Fink and J. Ingram, At. Data **4**, 129 (1972); D. Gregory and M. Fink, At. Data Nucl. Data Tables **14**, 39 (1974).
[8] J. Osterwalder, T. Greber, S. Hüfner, and L. Schlapbach, Phys. Rev. B **41**, 12 495 (1990).
[9] L.-G. Petersson, S. Kono, N. F. T. Hall, C. S. Fadley, and J. B. Pendry, Phys. Rev. Lett. **42**, 1545 (1979).
[10] D. A. Wesner, F. P. Coenen, and H. P. Bonzel, Phys. Rev. Lett. **60**, 1045 (1988).
[11] R. Fasel, P. Aebi, R. G. Agostino, D. Naumović, J. Osterwalder, A. Santaniello, and L. Schlapbach, Phys. Rev. Lett. **76**, 4733 (1996).
[12] R. Fasel and J. Osterwalder, Surf. Rev. Lett. **2**, 359 (1995).
[13] S. Schwegmann, H. Over, V. De Renzi, and G. Ertl, Surf. Sci. **375**, 91 (1996).
[14] T. Greber, O. Raetzo, T. J. Kreutz, P. Schwaller, W. Deichmann, E. Wetli, and J. Osterwalder, Rev. Sci. Intrum. **68**, 4549 (1997).
[15] S. Hüfner, J. Osterwalder, T. Greber, and L. Schlapbach, Phys. Rev. B **42**, 7350 (1990).
[16] D. J. Friedman and C. S. Fadley, J. Electron Spectrosc. Relat. Phenom. **51**, 689 (1990).
[17] J. Wider, T. Greber, E. Wetli, T. J. Kreutz, P. Schwaller, and J. Osterwalder, Surf. Sci. (unpublished).
[18] O. Knauff, U. Grosche, H. P. Bonzel, and V. Fritzsche, Mol. Phys. **76**, 787 (1992).